Appl Microbiol Biotechnol (2009) 82:271–278
DOI 10.1007/s00253-008-1735-4

BIOTECHNOLOGICALLY RELEVANT ENZYMES AND PROTEINS

The cyanide hydratase from *Neurospora crassa* forms a helix which has a dimeric repeat

Kyle C. Dent · Brandon W. Weber · Michael J. Benedik · B. Trevor Sewell

Received: 2 July 2008 / Revised: 24 September 2008 / Accepted: 25 September 2008 / Published online: 23 October 2008

Abstract The fungal cyanide hydratases form a functionally specialized subset of the nitrilases which catalyze the hydrolysis of cyanide to formamide with high specificity. These hold great promise for the bioremediation of cyanide wastes. The low resolution (3.0 nm) three-dimensional reconstruction of negatively stained recombinant cyanide hydratase fibers from the saprophytic fungus *Neurospora crassa* by iterative helical real space reconstruction reveals that enzyme fibers display left-handed D_1 $S_{5.4}$ symmetry with a helical rise of 1.36 nm. This arrangement differs from previously characterized microbial nitrilases which demonstrate a structure built along similar principles but with a reduced helical twist. The cyanide hydratase assembly is stabilized by two dyadic interactions between dimers across the one-start helical groove. Docking of a homology-derived atomic model into the experimentally determined negative stain envelope suggests the location of charged residues which may form salt bridges and stabilize the helix.

Keywords Cyanide · Nitrilase · 3d protein reconstruction · Cyanide hydratase

K. C. Dent
Department of Molecular and Cell Biology,
University of Cape Town,
Private Bag,
Rondebosch 7700, South Africa

B. W. Weber · B. T. Sewell (✉)
Electron Microscope Unit, University of Cape Town,
Private Bag,
Rondebosch 7700, South Africa
e-mail: Trevor.Sewell@uct.ac.za

M. J. Benedik
Department of Biology, Texas A&M University,
College Station, TX 77843-3258, USA

Introduction

The generation of cyanide containing waste results from cyanide utilization in a variety of applications, spanning such diverse industries as gold and silver mining, metal electroplating, polymer synthesis, and the production of fine chemicals, pharmaceuticals, dyes, and agricultural products (Baxter and Cummings 2006). Traditionally, chemical oxidation or stabilizations are used to treat these wastes; however, many groups have been studying the potential for bioremediation of such cyanide waste (O'Reilly and Turner 2003; Jandhyala et al. 2005).

The most promising approach utilizes cyanide degradation by enzymes belonging to the nitrilase family (Pace and Brenner 2001). These microbial nitrilases are a family of hydrolytic enzymes found in the cytoplasm of diverse bacterial and fungal genera. While there is notable conservation of sequence and quaternary structure, they differ primarily in their substrate range. The conversion of cyanide occurs in two different ways. Hydrogen cyanide is either converted to formic acid and ammonia by the cyanide dihydratases (CynD) or it is converted to formamide by the cyanide hydratases (CHT) (O'Reilly and Turner 2003). In an accompanying paper (Basile et al. 2008), we describe the characterization of new members of the cyanide hydratase family and their comparison to enzymes previously characterized. Engineering improved enzymes for such direct applications is one goal of our work (Wang and Benedik, personal communication). To that end, we are creating structural models of these enzymes.

Crystal structures of two classes of related proteins with known activities, namely the D-amino acid carbamoylase (Nakai et al. 2000) and several amidases (Kimani et al. 2007; Hung et al. 2007; Andrade et al. 2007), have been determined. The nitrilase enzyme family is characterized by

their topologically distinct structural architecture (CATH 3.60.110.10) and their conserved active site triad comprising a glutamic acid, a cysteine, and a lysine (Brenner 2002). Monomers have a αββα sandwich fold, and these associate across the "A surface" (Sewell et al. 2003) to form a αββα:αββα eight-layered dimer which is the basic unit of higher order oligomeric association. The dimers associate in different ways to form a variety of different homo-oligomeric assemblies including spirals and helices such as the 14 monomer spirals in the case of the CynD from *Pseudomonas stutzeri* (Sewell et al. 2003). In the case of the nitrilase from *Rhodococcus rhodochrous* J1, the situation is more complicated and differs from the situation in CynD. The short length spirals apparently undergo an autolysis, removing 39 C-terminal amino acids, which causes them to form long helices built on similar principles to the CynD spirals (Thuku et al. 2007).

The details of the mechanism of cyanide degradation have not been elucidated but evidence (Stevenson et al. 1992) exists that a thioimidate intermediate is formed by a nucleophilic attack of the active site cysteine on the hydrogen cyanide. This is then hydrolyzed with the formation of ammonia and an acyl intermediate in the case of CynD or formamide in the case of the cyanide hydratases. Presumably, subtle changes in the detailed configuration of the active site dictate whether the ammonia or the formamide is a better leaving group (Jandhyala et al. 2005), thereby defining whether the enzyme is a cyanide dihydratase or a cyanide hydratase.

In the case of the nitrilase from *R. rhodochrous* J1, substantial work (Nagasawa et al. 2000; Thuku et al. 2007) has linked enzyme activity to the formation of a spiral or helical oligomer. However, the formation of spirals or helices does not appear to be obligatory throughout the family, and indeed, DCase from *Agrobacterium* species is active as a tetramer (Nakai et al. 2000; Wang et al. 2001), several amidases form active hexamers having D3 symmetry, and there is reported an active nitrilase dimer from *Pyrococcus abyssi* (Mueller et al. 2006). On the basis of the crystal structure of the amidase, it is postulated (Kimani et al. 2007) that the loop containing a glutamate which may be responsible for catalyzing the hydrolysis of the acyl intermediate is moved into position by the formation of the spiral and that this, in turn, may explain the need for helix formation. In this context, there is clearly a need to understand the basis of the stabilization of the oligomeric helix.

In the accompanying paper (Basile et al. 2008), we have demonstrated the presence of a hitherto uncharacterized CHT from *Neurospora crassa* which has properties making it most suitable for biotechnological applications in cyanide remediation. Knowledge of the structures of these enzymes can inform their applications. For example, long helices may be more easily immobilized than smaller soluble dimers. Furthermore, modeling of the oligomers based on the structure of homologs can inform studies of the stability of the enzymes and possibly lead to the identification of sites for cross-linking and, hence, increasing the stability of the enzyme. With this in mind, we have determined the three dimensional structure of *N. crassa* CHT by negative stain electron microscopy and iterative, real space, helical reconstruction. We have also docked a model based on the structures of the known homologs into the negative stain envelope and have thus been able to build a hypothesis about which residues are involved in stabilizing the helical structure.

Materials and methods

Expression

The pET26b construct p3460, encoding the cyanide hydratase cDNA gene from *N. crassa* having 351 amino acids and having a molecular weight of 39.5 kDa (Basile et al. 2008), was used to transform competent *E. coli* BL21 (λDE3) pLysS cells by electroporation. Transformed cells were grown in Luria–Bertani broth at 37°C. Chloramphenicol and kanamycin were added to a final concentration of 50 μg/ml each. Expression of the recombinant cyanide hydratase gene was initiated in fresh cultures which had entered exponential growth phase (OD_{600} of 0.3) by the addition of isopropyl thiogalactose to the culture medium to a final concentration of 1 mM. Cultures were induced for 3 h, following which the cells were pelleted by centrifugation. The pellet was resuspended in 50 mM Tris/Cl buffer containing 100 mM NaCl pH 8.0 and sonicated on ice for a total period of 4 min. The lysate was then clarified of cell debris by centrifugation. Protein was precipitated with ammonium sulphate at 4°C. The purity of the protein of interest from each purification step was monitored by 10% *w/v* acrylamide sodium dodecyl sulfate polyacrylamide gel electrophoresis (Laemmli 1970) stained with Coomasie blue R250. Activity against cyanide was confirmed for each fraction of interest by the picric acid activity assay (Fisher and Brown 1952).

Protein purification

Protein fractionation by column chromatography was performed at room temperature using buffers which had been membrane filtered (0.45 μm) and degassed under vacuum for 20 min. Ammonium sulphate fractions containing the protein of interest were redissolved in 50 mM Tris buffer containing 100 mM NaCl pH 8.0, pooled, filtered using a 0.45-mm filter, and loaded onto a Q-

Sepharose QXL anion exchange column (GE Healthcare). Proteins were eluted with a linear salt gradient (100–1,000 mM NaCl) using a Waters Delta Prep 3000 Chromatography System. Anion exchange fractions containing the protein of interest were pooled and concentrated using a 50-ml stirred ultrafiltration cell (Amicon Corporation) using a 10-kDa exclusion membrane (Millipore PM10). The concentrate was filtered (0.22 μm) and loaded onto a prepacked 60×1.6-cm Sephacryl 300 HR gel filtration column (Amersham Biosciences), which had been equilibrated with two column volumes of Tris/HCl buffer containing 200 mM NaCl pH 8.0 at a flow rate of 0.5 ml/min. The elution was monitored at a wavelength of 280 nm (Gilson UV/VIS-151). Protein concentration was measured using the method of Bradford (1976) with bovine serum albumin as a standard.

Molecular mass determination

The relative molecular weight (M_r) of the native protein complex was determined by analytical scale size exclusion high performance liquid chromatography using a TSK-GEL G5000PW$_{xl}$ gel filtration column (Tosoh Bioscience) equilibrated with 50 mM Tris/HCl buffer containing 200 mM NaCl pH 8.0. Proteins were detected at 280 nm (Gilson UV/VIS-151). The column was calibrated with bovine thyroglobulin (670 kDa), bovine gamma-globulin (158 kDa), ovalbumin (44 kDa), horse myoglobin (17 kDa), vitamin B_{12} (1.35 kDa; BioRad Gel Filtration Standard) with acetone added to indicate total volume. V_t and V_o were 13.1 ml and 5.2 ml, respectively.

Negative stain electron microscopy

The chromatographic fraction of interest was diluted using Tris/HCl buffer containing 100 mM NaCl pH 8.0 to a concentration of ~0.02 mg/ml and 3 μl applied to a carbon film on a copper grid which had been glow discharged in nitrogen gas. Samples were stained with 2% uranyl acetate.

Grids were inspected at a magnification of 50,000 using a Leo 912 TEM. Low dose micrographs (110) were recorded with a Proscan 2048×2048 pixel CCD camera and TVIPS software. The calibrated sampling on the CCD was 2.28 Å/pixel. All micrographs were screened for unacceptable defocus or astigmatism at the time of capture (by computational diffraction analysis) and recorded in RAW format.

Image processing

Unless otherwise stated, all image (2D) and volume (3D) manipulations were performed using the SPIDER software package (Frank et al. 1996). Visual inspection of 2D images was performed using either V2 or BOXER of the EMAN suite (Ludtke et al. 1999), while inspection of 3-D volumes was performed with either WEB (of the SPIDER package) or UCSF Chimera (Petterson et al. 2004). Straight intact fibers were windowed into 256×256 pixel (~584 Å length) segments with a 10-pixel overlap using BOXER. This resulted in 853 images which were Gaussian band-pass filtered in Fourier space with radii of 1/270 and 1/15 Å and then normalized in real space. The average power spectrum was calculated as the sum of the individual power spectra of the images (Wang et al. 2006).

Three-dimensional reconstruction

Three-dimensional reconstruction was achieved using the iterative helical real space reconstruction (IHRSR; Egelman 2000). Starting models were either a 12-nm-diameter featureless cylinder or a fiber generated by applying the helical symmetry operators to the homology model. All parameters indicative of correct alignment were monitored during the reconstruction. Resolution of the final model was calculated using the method of Yang et al. (2003). As a further check on the plausibility of the model, the power spectrum of the model was compared with the average power spectrum of the original images.

Comparative modeling and docking

Selection of templates for homology modeling and alignment of the sequence to the template was assisted by mGenTHREADER (Jones 1999; McGuffin and Jones 2003). Homology models of the cyanide hydratase dimer were generated using MODELLER (Sali and Blundell 1993; Fiser and Sali 2003). The energy of the models was minimized but no attempt was made to model loop insertions. Accuracy of each model was evaluated by superimposition of the template structures using ALIGN (Cohen 1997) and visualization with UCSF Chimera. Side chain packing was then optimized using SCWRL (Bower et al. 1997) and a single model selected on the basis of stereochemical consistency.

The selected model was aligned so that the dimer axis lay along the x axis. Models were rotated azimuthally around this axis and translated along the axis by varying amounts. Helical symmetry was then applied to produce a nine-dimer model. These helical atomic models were docked into the map using contour-based cross-correlation-assisted rigid-body docking with CoLoReS from the SITUS package (Chacon and Wriggers 2002). The correlation coefficient was used to decide the radius and azimuthal angle which produced the best fit to the experimental density. The threshold density was specified such that density enclosed the expected protein volume. The docking of the helical model with the highest correlation to the three-dimensional volume was visualized using UCSF Chimera.

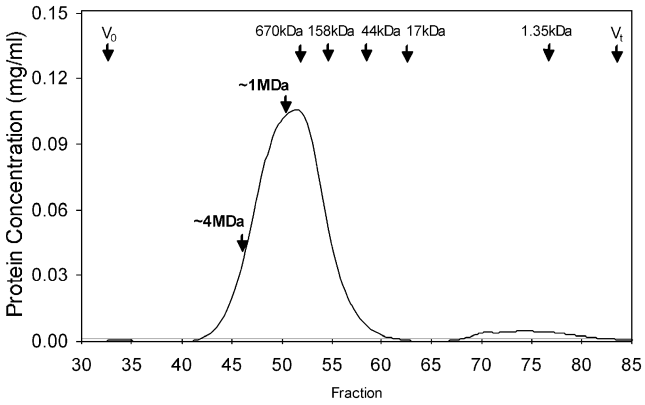

Fig. 1 Elution of recombinant *N. crassa* cyanide hydratase from a Tosoh TSK-GEL G5000PW$_{xl}$ gel filtration column monitored by absorbance at 280 nm. The entire eluted peak showed cyanide hydratase activity which was commensurate with the protein concentration

Results

Gel filtration chromatography

Protein was eluted from the gel filtration column in a broad range spanning 8 MDa to 80 kDa. The activity coincided with the location of the peak (Fig. 1).

Electron microscopy

Electron microscopy confirmed that the material eluted from the gel filtration column contained a single protein which formed fibrous oligomers with a diameter of 13 nm but with lengths ranging from approximately 1 μm at the leading edge of the peak to having approximately the same length and diameter at the trailing edge (Fig. 2). The range of lengths was found to be highly variable in different preparations suggesting that the fibers are susceptible to dissociation by mechanical shearing.

Three-dimensional reconstruction

The average power spectrum (Fig. 3a) produced from the selected vertically aligned fibers had visible layer lines corresponding to axial spacings of 12.2, 7.3, 5.2, 3.6, and 3.0 nm. These were interpreted as having Bessel orders of 6, 1, 4, 2, and 3, respectively. This indexing suggested 11 repeating units in two turns in a one-start helix having a pitch of 7.3 nm. Following the handedness determinations for similar nitrilase fibers from closely related species (Jandhyala et al. 2003; Woodward et al. 2008), it was assumed that the one-start helix is left handed. This suggested starting values of the helical twist per repeating unit ($\Delta\varphi$) of −65.5° and rise per repeating unit (Δz) of 1.3 nm for the IHRSR iterations. Reconstructions starting from these values and a number of other close values utilizing two different starting models always converged on values of $\Delta\varphi$=−66.67 and Δz=1.36 nm after about five cycles of iteration. This symmetry which has 27 repeating units in five turns also accounts for the observed power spectrum and can be described as D_1 $S_{5.4}$ (Makowski and Caspar 1980). It should be noted that convergence to different symmetry values was obtained for several different starting symmetries suggested by alternative indexing schemes but these produced implausible reconstructions. After convergence, a twofold symmetry axis perpendicular to the fiber axis was located. This symmetry was imposed on the reconstruction. This was justified because the reconstruction demonstrated clear symmetry even if none were imposed, and the fact that the repeating unit was a dimer, which can be clearly recognized in the reconstruc-

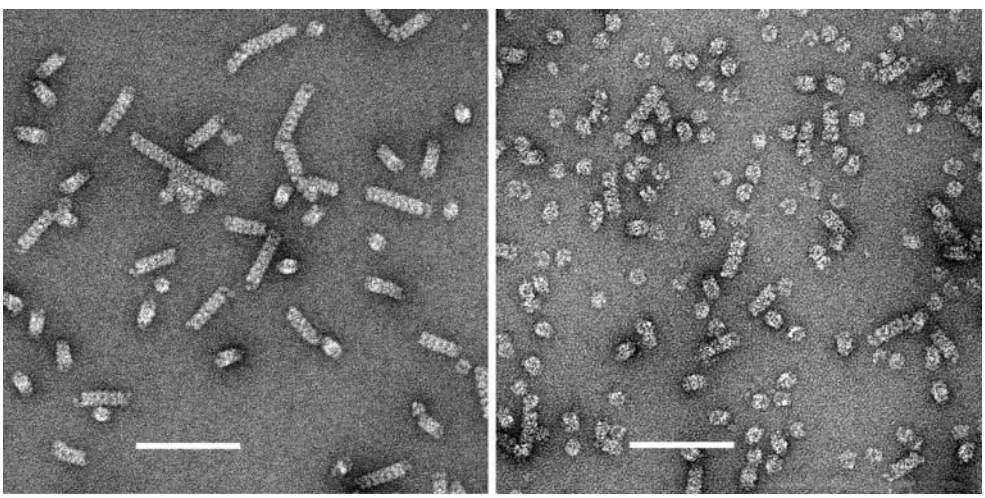

Fig. 2 Electron micrographs of negatively stained recombinant *N. crassa* cyanide hydratase fibers taken from **a** fraction 46 and **b** fraction 50 of the analytical gel filtration column. The *scale bar* indicates 100 nm

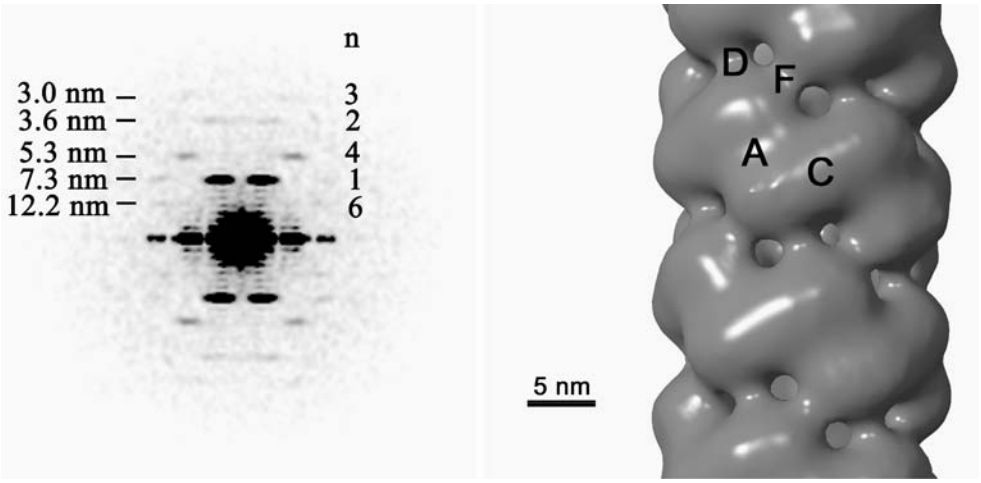

Fig. 3 **a** The average power spectrum of the 853 selected aligned images. *Five layer lines* corresponding to the spacings shown on the left are visible. These are interpreted as being of the Bessel order shown on the right. **b** The three-dimensional reconstruction of the density from the images using the iterative helical real space method. The locations marked *A*, *C*, *D*, and *F* are the interfaces between subunits. *Lines* between points of type A and D and between points of type C and F, passing through the helix and normal to it, are dyad axes. The left-handed one-start helix is formed by the subunits associating across interfaces A and C. The interactions across the groove at F and D stabilize the helix. The surface depicted has a volume of 4,048 nm^3 which encloses 42.7 dimers each having a molecular mass of 79 kDa. We assume that protein has a density of 0.83 kDa/nm^3

tion as having its symmetry axis perpendicular to the fiber axis. The reconstruction after convergence and the imposition of twofold symmetry is shown in Fig. 3b. The resolution of the reconstruction was 3 nm. Connectivity between the subunits can clearly be seen in the reconstruction. The left-handed one-start helix has two different subunit interfaces, both located on twofold axes. These are labeled A and C on Fig. 3b. Opposite each of these interfaces, located on the other side of the helix, there is connectivity across the groove. Thus, opposite A, the interaction is labeled D and opposite C, it is labeled F.

Interpretation of the reconstruction

Alignment of the sequence of *N. crassa* cyanide hydratase to the sequences of crystallographically determined members of the nitrilase superfamily was obtained from GenTHREADER (Jones 1999) and slightly modified by hand (Fig. 4). This enabled a model of the dimer to be built with MODELLER (Sali and Blundell 1993). The model had many features in common with those derived by Sewell et al. (2003, 2005) and Thuku et al. (2007) and is not shown. A possible improvement of the models presented previously is that the C-terminal region is visible in the structure of the amidase from *Geobacillus pallidus* (2plq, Kimani et al. 2007). If the structure of the amidase in this region is assumed to be similar to that of the cyanide hydratase, then it is predicted that after α7 (i.e., residue 295), the polypeptide chain associates with the subunit which is paired across the A surface, first interacting in the region of the C surface and then returning to the region of the A surface. In doing so, it forms an interlock which possibly increases the stability of this interface. In addition, the structure of the β-alanine synthase from *Drosophila melanogaster* (2vhi and 2vhh, Lundgren et al. 2008) provides a basis for modeling the C surface that was not previously available.

Since the twofold axis of the dimer must coincide with the corresponding dyad axis of the reconstruction, the docking of the model into the reconstruction is reduced to having only two degrees of freedom, a radial translation and an azimuthal rotation about the radius. A range of the space, in which these two coordinates were systematically varied, was explored. The docking of the optimal nine-dimer model to the reconstructed density is shown in Fig. 5. It was found that the threshold specified influenced the details of the fitting, and therefore, a threshold that enclosed the expected molecular mass was chosen.

The A surface interaction in the helix can be identified as the conserved dimer interface (involving the two helices α5 and α6) which occurs in all the homologs of which the structure has been determined. The other surfaces have only been visualized in electron microscopic reconstructions, and there is at present no crystallographic evidence to support the detailed placement of atoms. The model we propose must be therefore be seen as a guide for future experimentation. In the case of the C surface, we propose that the density is filled, by the residues in the two insertions reported previously (Sewell et al. 2003): 56–62, for which no good model currently exists, and 237–251, which can now be modeled on the β-alanine synthase structure, 2vhi, as well as by the residues in the carboxy-

```
                                          <D>                          *          <--C->
NCRACH    1:--------MVLTKYKAAAVTSEPCWFD----LEGGVRKTIDFINEAGQA---GCKLVAFPEVWIPG-YPYWMWKVTYQQSLPMLKKYRENAMAVDS
1J31      1:------------MVKVGYIQM-EPKIL---ELDKNYSKAEKLIKEASKE---GAKLVVLPELFDTG-YN--------FESREEVFDVAQQIPE--G
1ERZ      1:----------TRQMILAVGQQGPIARAE--TREQVVVRLLDMLTKAAS---RGANFIVFPELALTTFFPRWH-------FTDEAELDSFYETEMPG
2PLQ      1:-MRHGDISSSHDTVGIAVVNYKMPRLHTKAEVIENAKKIADMVVGMKQGLP-GMDLVVFPEYSTMGIMY-------------DQDEMFATAASIPG
2VHI     64:FTAREEQTRKRRIVRVGAIQNSIVIPTTAPIEKQREAIWNKVKTMIKAAAEAGCNIVCTQEAWTMPFAFCTREKF-------PWCEFAEEA-E-NG
                        <--β1-->            <------α1------->   <-β2->                          <--α2-->

                <D>   <F>                                        **                 <*C>    *          <F>
NCRACH   81:DEFRRIRRAARDNQIYVSLG-FAEIDH-----ATLYLAQALIDPTGEVINHRRKIKPT------------HVEKLVYGDGAGDTFMSVTPTELGRL
1J31     67:ETTTFLMELARELGLYIVAG-TAEK----SGN-YLYNSAVVVGPRG-YIGKYRKIHLF------------YREKVFFEPGDLG-FKVFDIG-FAKV
1ERZ     75:PVVRPLFEKAAELGIGFNLG-YAELVVEG-GVKRRFNTSILVDKSGKIVGKYRKIHLPGHKEYEAYRPFQHLEKRYFEPGDLG-FPVYDVD-AAKM
2PLQ     82:EETAIFAEACKKADTWGVFSLTGEKHEDHP-NKAPYNTLVLINNKGEIVQKYRKIIPWCP-----------IE--GWYPGDT-TY-VTEGPKGLKI
2VHI    147:PTTKMLAELAKAYRMVIIHS-ILERDMEHGE--TIWNTAVVISNSGRYLGKHRKNHIPRVGD--------FNESTYYMEGNTG-HPVFETEFG-KL
            <-----α3-----> <---β3-->           <--β4->      <-β5->                                <β6><-α4><

                 *     <----A---->                                <-----A----->              <-------C------>
NCRACH   159:GQLNCWENMNPFLKSLNVSMGEQIHIAAWPIYPGKETLKYPDPATNVADPASDLVTPAYAIETGTWTLAPFQRLSVEGLKKNTPEGVEPETDP-ST
1J31     142:GVMICFDWFFPESARTLALKGAEIIAHPANLV--------------MP-YAPRAMPIRALENRVYTITADRVGEERG----------------LK
1ERZ     167:GMFICNDRRWPEAWRVMGLRGAEIICGGYNTPTHNPPV---PQHDHLTSFHHLLSMQAGSYQNGAWSAAAGKAGMEEN----------------CM
2PLQ     162:SLIVCDDGNYPEIWRDCAMKGAELIVRCQGYMYP-------------AKEQQIMMAKAMAWANNTYVAVANATGFDGV----------------YS
2VHI     230:AVNICYGRHHPQNWMMFGLNGAEIVFNPSATIGRLS-----------EPLWSIEARNAAIANSYFTVPINRVGTEQFPNEYTSGDGNKAHKEFGP
            β7->       <---α5-->   <-β8->                    <------α6------>  <-β9-> <-β10>               <β

                *                                                  <-------C------><---------A---------->
NCRACH   254:YNGHARIYRPDGSLVVRPDK-DFDGLLFVDIDLNECHLTKALADFAGHYM-R-PDLIRLLVDTSRKELVTEVDRNGGIVQYSTRERLGLNTPLEND
1J31     206:FIGKSLIASPKAEVLSIASETE-EEIGVVEIDLNLARNKRLNDMNDIFKDRREEYYFR-----------------------------------
1ERZ     244:LLGHSCIVAPTGEIVALTTTLE-DEVITAAVDLDRCRELRE-H-IFNFKQHRQPQHYGLIAEL---------------------------------
2PLQ     229:YFGHSAIIGFDGRTLGECGT-EENGIQYAEVSISQIRDFRKNAQSQNHLFKLLHRGYTGLINSGEGDRGVAECPFDFYRTWVLDAEKARENVEKIT
2VHI     314:FYGSSYVAAPDGSRTPSLSR-DKDGLLVVELDLNLCRQVKDFRWG-FRMTQRVPLYAESFKKASEHGFKPQIIKET
            11>  <β12>    <β13>      <-β14--><--α7-->    <-α8>          <α9>              <α10> <---α11--->


NCRACH   347:KEGKK-----------
2PLQ     324:RSTVGTAECPIQGIPNE
```

Fig. 4 The alignment of the sequence of the cyanide hydratase from *N. crassa* (*NCRACH*) with the sequences of the four homologs, of which the crystal structures have been determined and used in the modeling. The catalytic triad residues are highlighted in *black*. The 12 residues that are identical in all four sequences are marked with an *asterisk*. The *letters in the upper row* denote the sequence segments predicted to be located at the interfaces. The predicted structural elements in the cyanide hydratase are indicated in the *lower row*. The structures used were the hypothetical protein PH0642 from *Pyrococcus horikoshii* (1j31, Sakai et al. 2004), the *N*-carbamyl-D-amino acid amidohydrolase from *Agrobacterium* sp. strain KNK712 (1erz, Nakai et al. 2000), the amidase from *Geobacillus pallidus* (2plq, Kimani et al. 2007), and the β-alanine synthase from *Drosophila melanogaster* (2vhi, Lundgren et al. 2008)

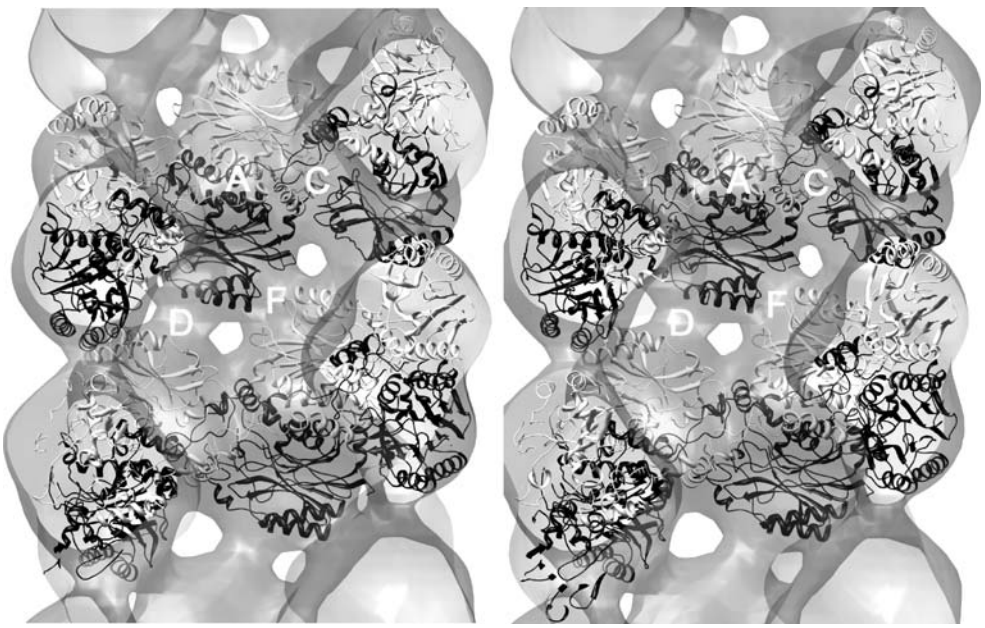

Fig. 5 Stereoview of the docked model. The molecular envelope is rendered as transparent and only the rear half of the fiber is shown. Subunits are shown alternately as *black and white* and are rendered as ribbons. The interfaces *A*, *C*, *D*, and *F* are labeled

terminal region (305–320) which can now be modeled based on the amidase structure, 2plq. Most of the carboxy-terminal region is located on the inside of the oligomeric helix.

The docking places a number of charged residues in proximity on opposite sides of the groove at locations D and F (Fig. 5). These could potentially interact forming stabilizing interactions across the groove. In particular, the model predicts that E21 faces R84 and R85 across the groove at D and could lead to the formation of a pair of salt bridges by interacting with either one of them. Similarly, R91 and E154 face one another at F. The small active site opening is located between the A and C surfaces with access at an angle about 30° to the helix axis.

Discussion

In the accompanying paper, we described the characterization of new cyanide hydratases enzymes from the saprophytic fungi *N. crassa* and *Aspergillus nidulans* and a comparison of them to known members of this nitrilase family with regard to properties relevant to bioremedation. The *N. crassa* cyanide hydratase was the most promising of these.

The structure of the *N. crassa* cyanide hydratase fiber has features in common with those of the C-terminal truncated nitrilase from *R. rhodochrous* J1 but it also has obvious differences. The dimer motif is clearly visible in the 3-nm resolution reconstruction and, in common with the nitrilase, the carboxy-terminal region is located on the inside of the fiber. However, the helical twist operator, $\Delta\varphi$, is −66.67° as opposed to −73.65° in the case of the nitrilase. This results in a helix with a greater diameter which, unlike the nitrilase, can accommodate the entire carboxy-terminal region of the expressed protein. This explains how the CHT fibers can be formed in the absence of proteolysis, unlike the nitrilase which exists as inactive dimers that can associate into active 480-kDa complexes under certain circumstances. Only when the 39 C-terminal amino acids of the nitrilase from *R. rhodochrous* J1 are lost due to autolysis are stable fibers formed. The CHT fibers were fragile and easily sheared, but we saw no evidence of the multistate system which occurs in the case of the nitrilase from *R. rhodochrous* J1.

The interaction across the groove at the D surface is similar to that observed in the case of the *R. rhodochrous* J1 nitrilase but an additional interaction at the F surface is visible. Indeed, the sequences of all helix forming homologs that have been investigated suggest that potential ion pairs exist in the helices that form the D surface. The F surface interaction, reported here, seems to involve a residue on the carboxy-terminal end of the α3 helix, opposite to that involved in the D surface, interacting with a residue in the outer surface bend leading to strand β7. This β strand is connected at its other end to the active site cysteine.

Our model includes information from the recently published series of amidase structures (Kimani et al. 2007; Hung et al. 2007; Andrade et al. 2007) which have revealed the detailed structure of the C-terminal region of a homologous enzyme. The docking places the sections 304–323 at the C interface and raises the possibility that amino acids in this region could interact to contribute to this surface. The high sequence variability in this part of the molecule suggests a greater conformational diversity than that of the αββα fold. Therefore, the specific interactions predicted may be unreliable; however, its location in the helix forming interface is consistent with the loss of activity on truncation of the C terminus previously reported by us in the case of the cyanide dihydratases from *P. stutzeri* AK61 and *B. pumilus* C1 (Sewell et al. 2005). While the *P. stutzeri* enzyme loses activity even with a small C-terminal deletion, the CynD from *B. pumilus* C1 can tolerate the removal of up to 28 residues from the C-terminal without destroying activity. This suggests to us that stabilization of the fragile fibers could be readily achieved by increasing the strength of interactions in this region, which is otherwise dispensable. It may also be possible to stabilize the helix through mutation at the D and F surfaces, for example, by increasing the number of interacting charged residues. Such stabilization is desirable as cyanide remediation of industrial wastewaters is often performed under conditions of high pH and other environmental insults.

Acknowledgements We thank Professor Edward H. Egelman for his assistance with the IHRSR programs and interpretation of the helical power spectrum, Mohammed Jaffer for assistance with the electron microscope, Dr. Arvind Varsani for his assistance with expression, and the Carnegie Corporation of New York, the National Research Foundation, the University of Cape Town, the Texas Hazardous Waste Research Center, and the Robert A. Welch Foundation (A-1310) for financial support.

References

Andrade J, Karmali A, Carrondo MA, Frazão C (2007) Structure of amidase from *Pseudomonas aeruginosa* showing a trapped acyl transfer reaction intermediate state. J Biol Chem 282:19598–19605

Basile LJ, Willson RC, Sewell BT, Benedik MJ (2008) Genome mining of cyanide-degrading nitrilases from filamentous fungi. Appl Microbiol Biotechnol 80(3):427–435 doi:10.1007/s00253-008-1559-2

Baxter J, Cummings SP (2006) The current and future applications of microorganism in the bioremediation of cyanide contamination. Antonie Van Leeuwenhoek 90:1–17

Bower JM, Cohen FE, Dunbrack RL Jr (1997) Prediction of protein side-chain rotamers from a backbone-dependant rotamer library: a new homology modeling tool. J Mol Biol 267:1268–1282

Bradford M (1976) A rapid and sensitive method for the quantitation of microgram quantities of protein utilizing the principle of protein-dye binding. Anal Biochem 72:248–254

Brenner C (2002) Catalysis in the nitrilase superfamily. Curr Opin Struct Biol 12:775–782

Chacón P, Wriggers W (2002) Multi-resolution contour-based fitting of macromolecular structures. J Mol Biol 317:375–384

Cohen GH (1997) ALIGN: a program to superimpose protein coordinates, accounting for insertions and deletions. J Appl Crystall 30:1160–1161

Egelman EH (2000) A robust algorithm for the reconstruction of helical filaments using single-particle methods. Ultramicroscopy 85:225–234

Fiser A, Sali A (2003) MODELLER: generation and refinement of homology-based protein structure models. Methods Enzymol 374:463–493

Fisher FB, Brown JS (1952) Colorimetric determination of cyanide in stack gas and waste water. Anal Chem 24:1440–1444

Frank J, Radermacher M, Penczek P, Zhu J, Li Y, Ladjadj M, Leith A (1996) SPIDER and WEB: processing and visualization of images in 3D electron microscopy and related fields. J Struct Biol 116:190–199

Hung CL, Liu JH, Chiu WC, Huang SW, Hwang JK, Wang W-C (2007) Crystal structure of *Helicobacter pylori* formamidase AmiF reveals a cysteine–glutamate–lysine catalytic triad. J Biol Chem 282:12220–12229

Jandhyala D, Berman M, Meyers PR, Sewell BT, Willson RC, Benedik MJ (2003) Cyn D, the cyanide dihydratase from *Bacillus pumillus*: gene cloning and structural studies. Appl Environ Microbiol 69:4794–4805

Jandhyala DM, Wilson RC, Sewell BT, Benedik MJ (2005) Comparison of cyanide degrading nitrilases. Appl Microbiol Biotechnol 68:327–335

Jones DT (1999) GenTHREADER: an efficient and reliable protein fold recognition method for genomic sequences. J Mol Biol 287:797–815

Kimani SW, Agarkar VB, Cowan DA, Sayed MF-R, Sewell BT (2007) The crystal structure of an aliphatic amidase from *Geobacillus pallidus* RAPc8: evidence for a fourth nitrilase catalytic residue. Acta Crystallogr D63:1048–1058

Laemmli UK (1970) Cleavage of structural proteins during the assembly of the head of bacteriophage T4. Nature 227:680–685

Ludtke SJ, Baldwin PR, Chiu W (1999) EMAN: semi-automated software for high-resolution single particle reconstructions. J Struct Biol 128:82–96

Lundgren S, Lohkamp B, Andersen B, Piskur J, Dobritzsch D (2008) The crystal structure of β-alanine synthase from *Drosophila melanogaster* reveals a homoactameric helical turn-like assembly. J Mol Biol 377:1544–1559

Makowski L, Caspar DLD (1980) The symmetries of filamentous phage particles. J Mol Biol 145:611–617

McGuffin LJ, Jones DT (2003) Improvement of the GenTHREADER method for genomic fold recognition. Bioinformatics 19:874–881

Mueller P, Egorova K, Vorgias CE, Boutou E, Trauthwein H, Verseck S, Antranikian G (2006) Cloning, overexpression, and characterization of a thermoactive nitrilase from the hyperthermophilic archaeon *Pyrococcus abyssi*. Protein Expr Purif 47:672–681

Nagasawa T, Wieser M, Nakamura T, Iwahara H, Yoshida T, Gekko K (2000) Nitrilase of *Rhodococcus rhodochrous* J1: Conversion into the active form by subunit association. Eur J Biochem 267:138–144

Nakai T, Hasegawa T, Yamashita E, Yamamoto M, Kumasaka T, Ueki T, Nanba H, Ikenaka Y, Takahashi S, Sato M, Tsukihara T (2000) Crystal structure of N-carbamyl-D-amino acid amidohydrolase with a novel catalytic framework common to amidohydrolases. Structure 8:729–737

O'Reilly C, Turner PD (2003) The nitrilases family of CN hydrolyzing enzymes—a comparative study. J Appl Microbiol 95:1161–1174

Pace HC, Brenner C (2001) The nitrilase superfamily: classification, structure and function. Genome Biol 2(1):REVIEWS0001

Pettersen EF, Goddard TD, Huang CC, Couch GS, Greenblatt DM, Meng EC, Ferrin TE (2004) UCSF Chimera—a visualization system for exploratory research and analysis. J Comput Chem 25:1605–1612

Sakai N, Tajika Y, Yao M, Watanabe N, Tanaka I (2004) Crystal structure of hypothetical protein PH0642 from *Pyrococcus Horikoshii* at 1.6A resolution. Proteins Struct Funct Bioinform 57:869–873

Sali A, Blundell TL (1993) Comparative protein modelling by satisfaction of spatial restraints. J Mol Biol 234:779–815

Sewell BT, Berman MN, Meyers PR, Jandhyala D, Benedik M (2003) The cyanide degrading nitrilase from *Pseudomonas stutzeri* AK61 is a two-fold symmetric, 14-subunit spiral. Structure 11:1–20

Sewell BT, Thuku RN, Zhang X, Benedik M (2005) The oligomeric structure of nitrilases: the effect of mutating interfacial residues on activity. Ann NY Acad Sci 1056:153–159

Stevenson DE, Feng R, Dumas F, Groleau D, Mihoc A, Storer AC (1992) Mechanistic and structural studies on *Rhodococcus* ATCC 39484 nitrilase. Biotechnol Appl Biochem 15:283–302

Thuku RN, Weber BW, Varsani A, Sewell BT (2007) Post-translational cleavage of recombinantly expressed nitrilase from *Rhodococcus rhodochrous* J1 yields a stable, active helical form. FEBS J 274:2099–2018

Wang W, Hsu W, Chien F, Chen C (2001) Crystal structure and site-directed mutagenesis studies of N-Carbamoyl-D-amino-acid amidohydrolase from *Agrobacterium radiobacter* reveals a homotetramer and insight into a catalytic cleft. J Mol Biol 306:251–261

Wang YA, Yu X, Yip C, Strynadka NC, Egelman EH (2006) Structural polymorphism in bacterial EspA filaments revealed by Cryo-EM and an improved approach to helical reconstruction. Structure 14:1–8

Woodward JD, Weber BW, Scheffer MP, Benedik MJ, Hoenger A, Sewell BT (2008) Helical structure of unidirectionally shadowed fibres of cyanide hydratase from *Gloeocercospora sorghi*. J Struct Biol 161:111–119

Yang S, Yu X, Galkin VE, Egelman EH (2003) Issues of resolution and polymorphism in single-particle reconstruction. J Struct Biol 144:162–171